Science & Technology Development Journal 2022, 25(3):2489-2496

Open Access Full Text Article

Original Research

Structural, electrical and thermoelectric characterizations of bismuth-doped ZnO ceramic material

Thang Minh Bui[1,2,3], Dai Cao Truong[2,4], Phung Y Nguyen[1,2,3], Anh Tuan Thanh Pham[1,2,*], Dung Van Hoang[1,2], Truong Huu Nguyen[1,2], Thang Bach Phan[1,2,4], Vinh Cao Tran[1,2]

ABSTRACT

Introduction: ZnO is a potential semiconductor material for thermoelectric (TE) applications at high temperature. In this study, doping Bi atoms aims to improve the power factor of ZnO ceramics. Based on the analyses of structural and TE properties, the enhancement in the Seebeck coefficient proves the benefit of Bi doping. **Methods:** ZnO and Bi-doped ZnO (BZO) ceramics were fabricated by a solid-state reaction at 1400°C in air. The Seebeck LSR-3 system measured both samples' TE properties, with a combined Hall effect at room temperature. The crystalline structure was analyzed through the X-ray diffraction (XRD) technique. **Results:** The XRD patterns show that all samples have polycrystalline hexagonal wurtzite structures. Although the crystallinity is enhanced, Bi doping significantly reduces the carrier concentration from 3.4×10^{19} to 1.1×10^{19} cm^{-3} at room temperature. As a result, at 500°C, the electrical conductivity, Seebeck coefficient, and power factor are 126 Scm^{-1}, -99 μVK^{-1}, and 124 $\mu Wm^{-1}K^{-2}$ for pure ZnO and 76 Scm^{-1}, -142 μVK^{-1}, and 165 $\mu Wm^{-1}K^{-2}$ for BZO ceramic, respectively. **Conclusion:** The power factor of Bi-doped ZnO is improved by 32% compared to pure ZnO at 500°C. The increase in the Seebeck coefficient is the main reason for the increase in the power factor.

Key words: Thermoelectric properties, ZnO ceramics, Bismuth doping, microstructure, power factor

[1]*Laboratory of Advanced Materials, University of Science, Ho Chi Minh City, Vietnam*

[2]*Vietnam National University, Ho Chi Minh City, Vietnam*

[3]*Faculty of Physics and Engineering Physics, University of Science, Ho Chi Minh City, Vietnam*

[4]*Center for Innovative Materials and Architecture (INOMAR), Ho Chi Minh City, Vietnam*

Correspondence

Anh Tuan Thanh Pham, Laboratory of Advanced Materials, University of Science, Ho Chi Minh City, Vietnam

Vietnam National University, Ho Chi Minh City, Vietnam

Email: pttanh@hcmus.edu.vn

History

- Received: 2022-05-08
- Accepted: 2022-10-03
- Published: 2022-10-15

DOI : 10.32508/stdj.v25i3.3935

Check for updates

INTRODUCTION

Thermoelectric (TE) materials can directly convert waste heat into electric energy thus, the efficiency of energy consumption is significantly enhanced[1]. In addition, they also have some advantages, including no fume emission and quietness[2]. One of the performances of TE materials is estimated by the power factor, PF = σS^2, where σ and S are the electrical conductivity and Seebeck coefficient, respectively. This quantity represents the energy harvesting ability[3]. Currently, traditional alloy materials have high-quality TE properties, such as Bi_2Te_3 [4] and Bi-Sb-Te[5]. However, these materials are limited by a short range of operation temperatures[6]. Therefore, the development of oxide materials is necessary to expand applications in a broad temperature range. Herein, ZnO is one of the promising oxide materials for TE modules at high temperature[7–9]. ZnO has some benefits, such as a wide bandgap of 3.37 eV at room temperature and the ability to easily control structural and electrical properties through doping[10]. In previous reports, to improve PF, many elements were chosen for doping into ZnO, typically the IIIA group (Al[11,12], Ga[13,14], In[15]), or synthesizing hybrid nanostructures, such as compositing ZnO with graphene[16,17]. However, due to the good Zn substitution of the IIIA elements, the good crystalline structure and a high carrier concentration normally strongly increase the thermal conductivity of ZnO films. To solve this problem, there have been some reports on other metallic dopants in ZnO, such as Bi[18], Sn[19], Sb[20], and Ni[21]. These transition metals have large ionic radii and heavy atomic masses, which are beneficial for increasing phonon scattering and thus reducing the thermal conductivity of ZnO. Nevertheless, these elements are also easy to segregate in secondary phases and grain boundaries due to their low solid solubility in ZnO[18,19]. It can significantly degrade the crystalline quality and thermoelectric performance of the host ZnO material.

In this work, bismuth (Bi) dopant is selected for investigation. Bi has a larger ionic radius (1.1 Å) than Zn (0.74 Å); however, it can still dissolve well in the ZnO network [22]. The results show that Bi doping has the potential to increase the thermoelectric power factor of ZnO without creating secondary phase segregation. As a result, the 2 at.% Bi-doped ZnO ceramic shows an enhancement in the thermoelectric power factor by 32% at 500°C compared to pure ZnO.

Cite this article : Bui T M, Truong D C, Nguyen P Y, Pham A T T, Hoang D V, Nguyen T H, Phan T B, Tran V C. **Structural, electrical and thermoelectric characterizations of bismuth-doped ZnO ceramic material**. *Sci. Tech. Dev. J.;* 2022, 25(3):2489-2496.

MATERIALS – METHODS

Both pure ZnO and Bi-doped ZnO (BZO) ceramics were prepared by a solid-state reaction in air. For the 2 at.% Bi-doped ZnO sample, a mixture of ZnO (99.9%, Merck), Bi_2O_3 (99.9995%, Alfa Aesar) powders, and 2^{nd}-distilled water were mixed and ground in a corundum mill pot for 5 hours by using a planetary ball milling apparatus (Ceramic Instrument). After that, the slurry was completely dried at 120°C for 24 hours to evaporate the water. By using a stainless-steel die with an inner diameter of 3 cm, the dried mixture was pressed under 14 MPa produced from a hydraulic compressor. Finally, the green compact bodies were sintered at 1400°C in air for 3 hours at a temperature acceleration rate of 5°C/min. After the sintering process, the pellets were polished by sandpapers with 400 and 1000 grit to remove surface contaminants.

The crystalline characteristics of the samples were determined by an X-ray diffraction system (Bruker D8-Advance) with a radiation source (= 0.154 Å), the θ-2θ configuration, and the 2θ region from 20° to 80°. The $10\times10\times1$ mm^3-sized pieces were used for measuring the electrical parameters (carrier concentration, mobility) by a Hall measurement system (Ecopia HMS-3000) at room temperature. Before the Hall measurement, the ohmic electrodes were soldered at four corners of the square pieces by indium-tin alloy. The temperature-dependent electrical conductivity, Seebeck coefficient, and thermoelectric power factor of the samples were simultaneously obtained from room temperature to 500°C by using a Linseis LSR-3 system. All the measurements were analyzed at least three times for repeatability and error margin calculation.

RESULTS

Figure 1 shows XRD patterns of pure ZnO and BZO ceramics. According to the JCPDS No. 36-1451 standard, the diffraction peaks represent the hexagonal wurtzite structure of ZnO. The intensity of the diffraction peaks increases significantly when Bi^{3+} is doped. In addition, small strange peaks appear at approximately 31.31° and 36.94° in the BZO sample. They can belong to the secondary -Bi_2O_3 phase or spinel in host ZnO due to the limited solid solution of Bi_2O_3 powder[22]. To consider the effect of Bi doping on the structure of ZnO, some crystallographic parameters were determined.

First, the mean crystal size D is defined by Scherrer's equation[8,9]:

$$D = \frac{0.9\lambda}{\beta\cos\theta} \quad (1)$$

where λ is the wavelength of CuKα X-ray radiation (0.154 nm), β is the full width at half maximum (FWHM) of the diffraction peaks, and is the Bragg diffraction angle.

Second, the lattice strain η is an important parameter that suggests the perfection degree of crystals, as given by[23,24]:

$$\eta\,(\%) = \frac{\beta}{4\tan\theta}\times 100\% \quad (2)$$

The mean crystal size and lattice strain of ZnO and BZO are listed in Table 1. The positions of preferred planes, including (100), (002), and (101), tend to shift toward lower 2θ angles. This can be explained by Zn^{2+} substitution of Bi^{3+} with a larger radius[22].

Third, the lattice constants of the samples are shown in Table 2, which can be estimated by the following equations[25,26]:

$$\alpha = \frac{\lambda}{\sqrt{3}\sin\theta_{(100)}} \quad (3)$$

$$c = \frac{\lambda}{\sin\theta_{(002)}} \quad (4)$$

where a and c are lattice constants along the a- and c-axes, respectively.

Figure 2 shows the electrical conductivity as a function of temperature. Generally, both samples behave as nondegenerate semiconductors because the electrical conductivity increases with temperature. At 500°C, the conductivities are found to be 126 Scm^{-1} and 76 Scm^{-1} for the ZnO and BZO ceramics, respectively. Over the range of room temperature – 500°C, the electrical conductivity of ZnO is degraded nearly 1.7 times by doping Bi.

To deeply consider the electrical properties, the charged carrier concentration and mobility of ZnO and BZO are listed in Table 3. The carrier concentration of the ZnO ceramic is 3.4×10^{19} cm^{-3}, which is larger than that of the BZO sample (1.1×10^{19} cm^{-3}). On the other hand, the mobility increases slightly from 16.7 cm^2/Vs (ZnO) to 18.2 cm^2/Vs (BZO). The results of electrical conductivity obtained from the LSR-3 and Hall measurements are reasonable. Thus, the reduction in electrical conductivity can be mainly attributed to the degradation of the carrier concentration.

Figure 3 shows the Seebeck coefficient as a function of temperature. All samples have negative Seebeck coefficients, suggesting n-type semiconductor behavior. The absolute Seebeck coefficient increases remarkably with temperature. At 500°C, the BZO ceramic obtains a maximum of -142 μVK^{-1}, which is an improvement of 70% compared to that of the ZnO sample (-99.34 μVK^{-1}).

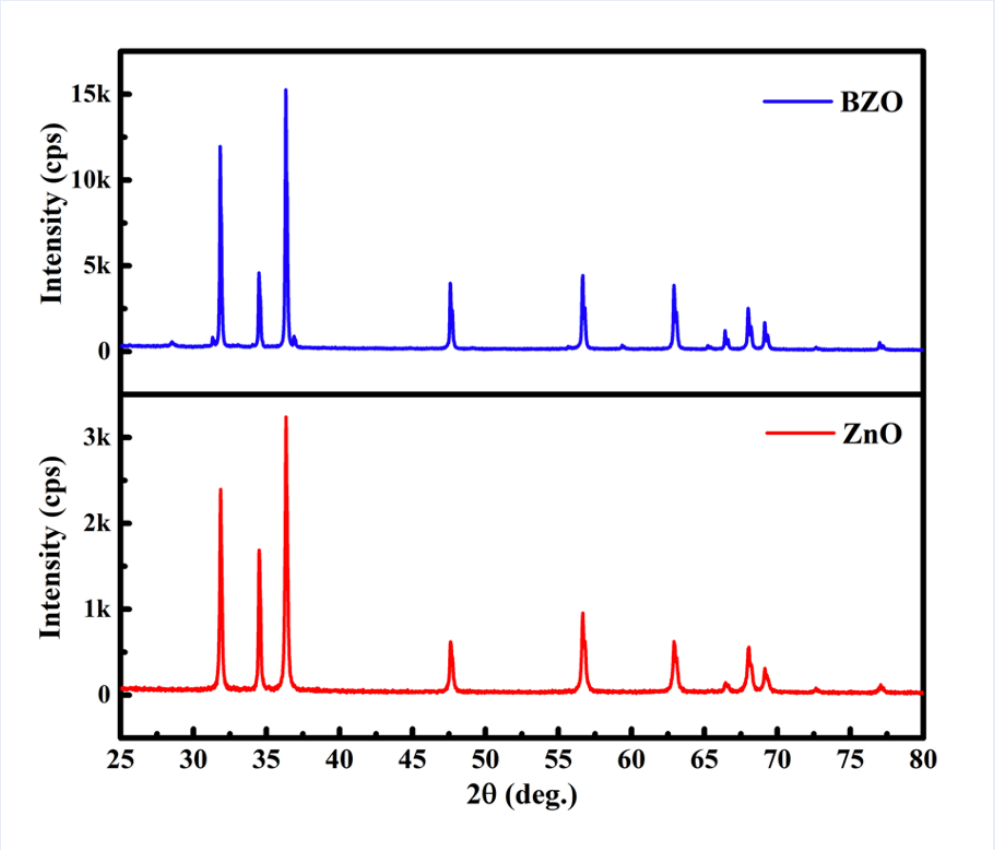

Figure 1: XRD patterns of pure ZnO (bottom) and BZO (top) ceramics. All the patterns are similar to the ZnO structure (JCPDS No. 36-1451).

Table 1: The calculations of mean crystal size and lattice strain along preferred orientations of ZnO and BZO ceramics.

Samples	ZnO			BZO		
Planes	(100)	(002)	(101)	(100)	(002)	(101)
2θ (^{o})	31.86	34.50	36.33	31.81	34.49	36.32
FWHM (^{o})	0.164	0.159	0.178	0.137	0.158	0.161
D (nm)	50.36	52.60	46.98	60.10	57.73	51.89
η (%)	0.250	0.222	0.233	0.210	0.221	0.214

Table 2: The lattice constants of ZnO and BZO ceramics.

Samples	a (Å)	c (Å)
ZnO	3.239	5.192
BZO	3.244	5.194

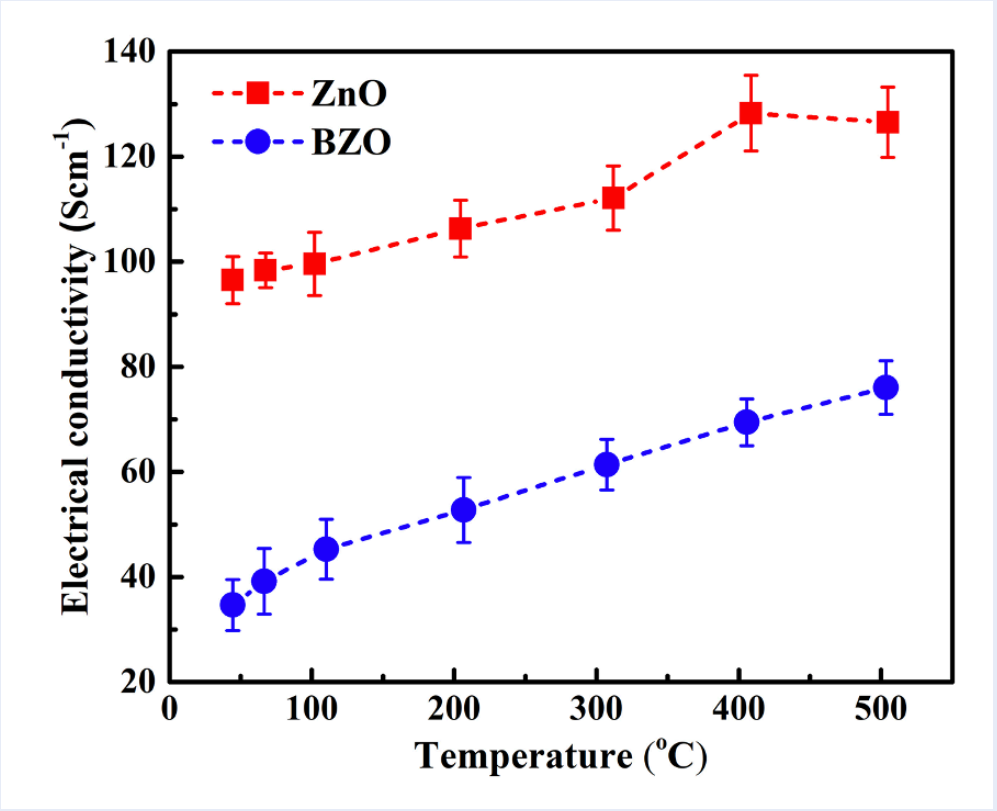

Figure 2: Dependence of electrical conductivity on temperature of pure ZnO (red squares) and BZO (blue circles) ceramics. The error margin of the conductivity is approximately 5%.

Table 3: Electrical parameters of ZnO and BZO ceramics at room temperature.

Samples	Hall measurement			LSR-3
	n (10^{19} cm^{-3})	μ ($cm^2V^{-1}s^{-1}$)	σ (Scm^{-1})	σ (Scm^{-1})
ZnO	3.4 ± 0.2	16.7 ± 0.3	90.8 ± 7.1	99.58 ± 6
BZO	1.1 ± 0.3	18.2 ± 0.5	32.0 ± 9.8	45.27 ± 5.72

Figure 4 shows the thermoelectric power factor as a function of temperature. The power factors of the two samples increase significantly with temperature. At 500°C, the PF of the BZO ceramic is found to be 165 $\mu Wm^{-1}K^{-2}$, which is enhanced by 32% compared to that of the ZnO ceramic (124 $\mu Wm^{-1}K^{-2}$). Although Bi doping reduces the electrical conductivity of the BZO sample, its Seebeck coefficient is improved. Therefore, the enhancement of PF is mainly contributed by the compensation of the Seebeck coefficient.

DISCUSSION

The BZO ceramic material has better crystallinity than ZnO due to the increased diffraction intensity, large crystal size, and reduced lattice strain along with the preferred (100), (002), and (101) orientations (Figure 1). The possible reason can come from the Zn^{2+} substitution of Bi^{3+} with a larger radius. In addition, the Zn^{2+} substitution of Bi^{3+} tends to shrink the unit cell of ZnO. Unexpectedly, the electrical conductivity of BZO is lower than that of the ZnO ceramic (Figure 2). The reduction in electrical conductivity is attributed to the decreased carrier concentration. It is well known that Bi dopants have many oxidation states, including Bi^{3+}, Bi^{2+}, Bi^{+}, and Bi^{0} [27,28]. Consequently, the existence of unexpected oxidation states (Bi^{2+}, Bi^{+}, and Bi^{0}) can destroy the electrical characteristics of ZnO. On the other hand, owing to the reduction in carrier concentration, the

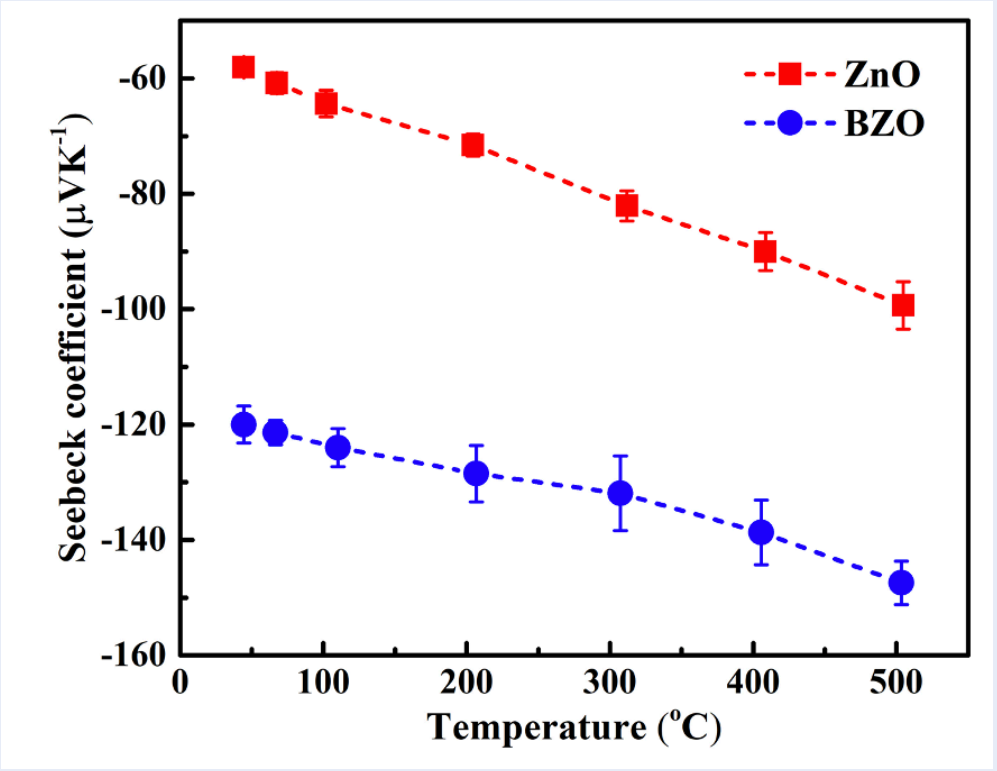

Figure 3: Dependence of the Seebeck coefficient on the temperature of pure ZnO (red squares) and BZO (blue circles) ceramics. The error margin of the Seebeck coefficient is approximately 5%.

Seebeck coefficient of the BZO ceramic is significantly enhanced (Figure 3). This trade-off can be described by the following equation [29–31]:

$$S = \frac{8\pi^2 k_B^2}{3eh^2} m_d^* T \left(\frac{\pi}{3n}\right)^{\frac{2}{3}} \quad (5)$$

where k_B is the Boltzman constant,e is the elementary charge, h is the Plank constant, m_d^* is the effective mass, T is the absolute temperature, and n is the carrier concentration. Through equation (5), S is proportional to $n^{-2/3}$. Consequently, the increased Seebeck coefficient compensates for the diminished electrical conductivity, leading to the enhanced TE power factor.

From the results, despite decreasing the electrical conductivity, Bi doping shows good potential for improving the thermoelectric power factor of the ZnO material due to a significant enhancement in the Seebeck coefficient. In the literature, there have been only a few studies on Bi-doped ZnO ceramic materials. Table 4 illustrates the comparison of the electrical and thermoelectric properties of the Bi-doped ZnO material reported previously. The Bi-doped ZnO obtained from this study has a much higher carrier concentration and mobility than other reports [18,32]. This is attributed to the good Zn substitution of Bi, which produces many free carriers and improves the crystalline structure of ZnO. As a result, the electrical conductivity is significantly enhanced, leading to an outstanding value of the power factor of $Zn_{0.98}Bi_{0.02}O$. However, to fully estimate the thermoelectric performance, the thermal conductivity must be determined. This quantity is not considered here and will be investigated in a future study.

CONCLUSION

In this work, the crystallographic, electrical, and thermoelectric properties of ZnO and 2 at.% Bi-doped ZnO are investigated. Through the XRD results, the Bi atoms incorporate well into the host ZnO network, which improves the crystalline structure and the carrier mobility of ZnO. However, because Bi has many oxidation states, Bi doping may damage the charged carrier concentration of ZnO. For the BZO ceramic, the electrical conductivity is reduced to 76 Scm^{-1}, while the Seebeck coefficient is increased to -142 μVK^{-1} at 500°C. As a result, the power factor is

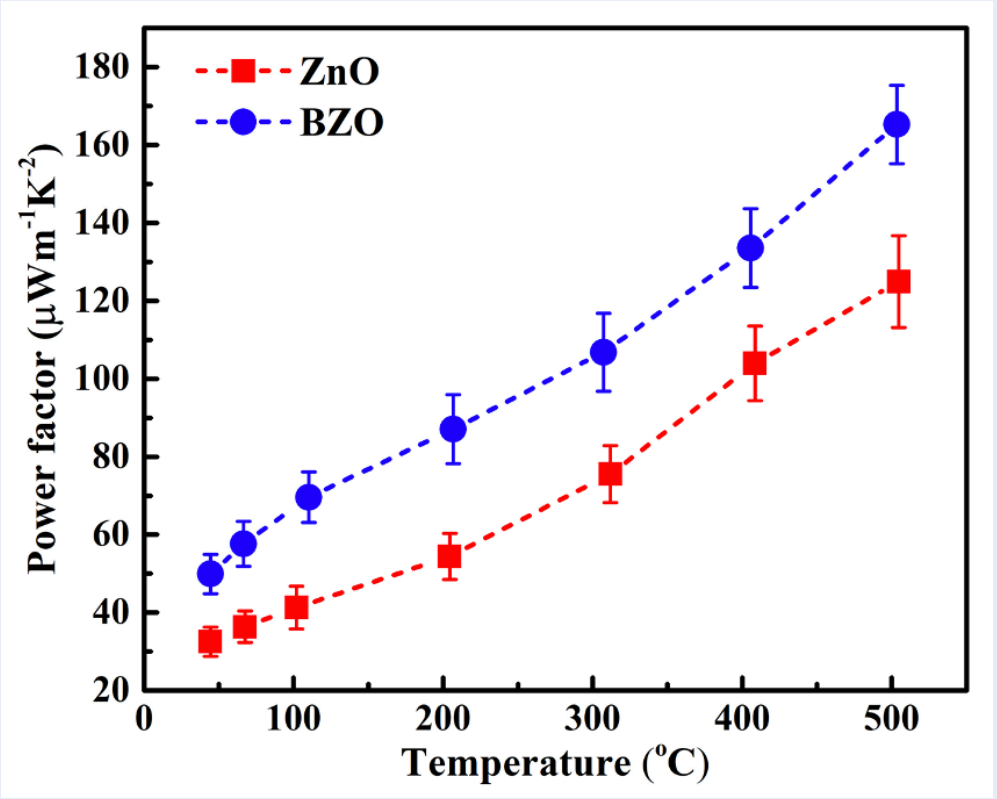

Figure 4: Dependence of the power factor on the temperature of pure ZnO (red squares) and BZO (blue circles) ceramics. The error margin of the power factor is less than 10%.

Table 4: Comparison of the electrical and thermoelectric properties of Bi-doped ZnO.

Composition	Method	n (cm^{-3})	μ (cm^2/Vs)	σ (S/cm)	S (μV/K)	PF (μW/mK^2)	Ref.
$Zn_{0.99}Bi_{0.01}O$	Microwaving/Solid-state reaction	~10^{15}	15	0.002	-520	0.054 (RT)	[18]
$Zn_{0.98}Bi_{0.02}O$	Spark plasma sintering	~10^{18}	10	2.5	-550	75.6 (700^{o}C)	[32]
$Zn_{0.98}Bi_{0.02}O$	Solid-state reaction	~10^{19}	18.2	76.1	-142	165 (500^{o}C)	This work

enhanced by 32% to 165 μW$m^{-1}K^{-2}$. This enhancement is contributed by optimizing the Seebeck coefficient rather than the electrical conductivity.

LIST OF ABBREVIATION

BZO: Bi-doped ZnO

PF: Power factor

RT: Room temperature

TE: Thermoelectric

XRD: X-ray diffraction

COMPETING INTERESTS

The authors declare that they have no competing interests.

AUTHOR CONTRIBUTIONS

Thang Minh Bui synthesized the samples and wrote the draft. Dai Cao Truong wrote the draft. Phung Y Nguyen prepared the samples. Anh Tuan Thanh Pham performed all the measurements and revised the manuscript. Dung Van Hoang and Truong Huu Nguyen took part in the discussion. Thang Bach Phan and Vinh Cao Tran act as scientific supervisors. All

the authors have approved the contents of the final version.

ACKNOWLEDGMENTS

This research is funded by University of Science, VNU-HCM under grant number T2021-35. The authors also acknowledge Faculty of Material Science and Technology, US (VNU-HCM) for Hall measurement, and INOMAR Center (VNU-HCM) for XRD Bruker D8-Advance and thermoelectric analysis Linseis LSR-3.

REFERENCES

1. Vogel-schäuble N, Romanyuk YE, Yoon S, Saji KJ, Populoh S, Pokrant S, et al. Thermoelectric properties of nanostructured Al-substituted ZnO thin films. Thin Solid Films 2012;520:6869-6875;Available from: https://doi.org/10.1016/j.tsf.2012.07.046.
2. Luo ZZ, Hao S, Cai S, Bailey TP, Tan G, Luo Y, et al. Enhancement of thermoelectric performance for n-type PbS through synergy of gap state and Fermi level pinning. J. Am. Chem. Soc. 2019;141:6403-6412;PMID: 30916942. Available from: https://doi.org/10.1021/jacs.9b01889.
3. Hoang DV, Pham ATT, Nguyen TH, Lai HT, Truong DC, Le TBN, et al. Tailoring orientation of microstructure for improving thermopower factor in Mg-doped CuCrO2 thick films. Appl. Phys. Lett.2022;120:063902;Available from: https://doi.org/10.1063/5.0079960.
4. Poudel B, Hao Q, Ma Y, Lan Y, Minnich A, Yu B, et al. High-thermoelectric performance of nanostructured bismuth antimony telluride bulk alloys. Science (80-.). 2008;320:634-638;Available from: https://doi.org/10.1126/science.1156446.
5. Lee KH, Kim S il, Kim HS, Kim SW. Band convergence in thermoelectric materials: theoretical background and consideration on Bi-Sb-Te alloys. ACS Appl. Energy Mater. 2020;3:2214-2223;Available from: https://doi.org/10.1021/acsaem.9b02131.
6. Huang Z, Zhao LD. Sb2Si2Te6: A robust new thermoelectric material. Trends Chem. 2020;2:89-91;Available from: https://doi.org/10.1016/j.trechm.2019.12.006.
7. Boumezoued A, Guergouri K, Barille R, Rechem D, Mourad Z. Synthesis and characterization of ZnO-based nano-powders: study of the effect of sintering temperature on the performance of ZnO-Bi2O3 varistors. J. Mater. Sci. Mater. Electron. 2021;32:3125-3139;Available from: https://doi.org/10.1007/s10854-020-05062-3.
8. Pham ATT, Luu TA, Pham NK, Ta HKT, Nguyen TH, Hoang DV, et al. Multi-scale defects in ZnO thermoelectric ceramic materials co-doped with In and Ga. Ceram. Int. 2020;46:10748-10758;Available from: https://doi.org/10.1016/j.ceramint.2020.01.084.
9. Truong DC, Pham ATT, Le OKT, Hoang DV, Nguyen TH, Ta HKT, et al. A comparative study on thermoelectric properties of ZnO bulks and thin films. Sci. Technol. Dev. J. 2020; 23: 788-794;Available from: https://doi.org/10.32508/stdj.v23i4.2458.
10. Fan P, Li Y, Zheng Z, Lin Q, Luo J, Liang G, et al. Thermoelectric properties optimization of Al-doped ZnO thin films prepared by reactive sputtering Zn-Al alloy target. Appl. Surf. Sci. 2013;284:145-149;Available from: https://doi.org/10.1016/j.apsusc.2013.07.070.
11. Trinh TQ, Nguyen TT, Vu DV, Le DH. Structural and thermoelectric properties of Al-doped ZnO thin films grown by chemical and physical methods. J. Mater. Sci. Mater. Electron. 2017;28:236-240;Available from: https://doi.org/10.1007/s10854-016-5516-z.
12. Wiff JP, Kinemuchi Y, Kaga H, Ito C, Watari K. Correlations between thermoelectric properties and effective mass caused by lattice distortion in Al-doped ZnO ceramics. J. Eur. Ceram. Soc. 2009;29:1413-1418;Available from: https://doi.org/10.1016/j.jeurceramsoc.2008.09.014.
13. Nguyen NHT, Nguyen TH, Liu Y, Aminzare M, Pham ATT, Cho S, et al. Thermoelectric properties of indium and gallium dually-doped ZnO thin films. 2016;8:33916-33923;Available from: https://doi.org/10.1021/acsami.6b10591.
14. Le OKT, Pham ATT, Nguyen TH, Hoang DV, Phan TB, Tran VC. Impacts of Ga doping on the structural and thermoelectric properties of ZnO bulks sintered by solid-state reaction. Sci. Technol. Dev. J. 2022;25:2432-2438;Available from: https://doi.org/10.32508/stdj.v25i2.3928.
15. Ullah M, Chunlei W, Su WB, Manan A, Ahmad AS, Rehman AU. Thermoelectric properties of indium-doped zinc oxide sintered in an argon atmosphere. J. Mater. Sci. Mater. Electron. 2019;30:4813-4818;Available from: https://doi.org/10.1007/s10854-019-00775-6.
16. Nam WH, Kim BB, Seo SG, Lim YS, Kim JY, Seo WS, et al. Structurally nanocrystalline-electrically single crystalline zno-reduced graphene oxide composites. Nano Lett. 2014;14:5104-5109;Available from: https://doi.org/10.1021/nl5018089.
17. Trinh TQ, Nguyen TT, Vu DV, Le DH. Microstructural analysis and thermoelectric performance of Ga-doped ZnO/reduced graphene oxide thin film nanocomposites. Ceram. Int. 2021;47:32033-32042;Available from: https://doi.org/10.1016/j.ceramint.2021.08.092.
18. Jood P, Mehta RJ, Zhang Y, Borca-Tasciuc T, Dou SX, Singh DJ, et al. Heavy element doping for enhancing thermoelectric properties of nanostructured zinc oxide. RSC Adv. 2014; 4: 6363;Available from: https://doi.org/10.1039/C3RA46813E.
19. Jacob J, Rehman U, Mahmood K, Ali A, Mehboob K, Ashfaq A, et al. Improved thermoelectric performance of Al and Sn doped ZnO nano particles by the engineering of secondary phases. Ceram. Int. 2020;46:15013-15017;Available from: https://doi.org/10.1016/j.ceramint.2020.03.031.
20. Yang Y, Pradel KC, Jing Q, Wu JM, Zhang F, Zhou Y, et al. Thermoelectric nanogenerators based on single Sb-doped ZnO micro/nanobelts. ACS Nano 2012;6:6984-6989;Available from: https://doi.org/10.1021/nn302481p.
21. Zhu BB, Chen C, Yao ZC, Chen JY, Jia C, Wang ZH, et al. Multiple doped ZnO with enhanced thermoelectric properties. J. Eur. Ceram. Soc. 2021;41:4182-4188;Available from: https://doi.org/10.1016/j.jeurceramsoc.2021.01.054.
22. Boumezoued A, Guergouri K, Barille R, Rechem D, Zaabat M, Rasheed M. ZnO nanopowders doped with bismuth oxide, from synthesis to electrical application. J. Alloys Compd. 2019;791:550-558;Available from: https://doi.org/10.1016/j.jallcom.2019.03.251.
23. Truong DC, Thaowonkaew S, Muthitamongkol P, Horprathum M, Kumar M, Le TBN, et al. Relaxation of residual stress-controlled thermopower factor in transparent-flexible Ti-doped ZnO thin films. Ceram. Int. 2022;48:2605-2613;Available from: https://doi.org/10.1016/j.ceramint.2021.10.043.
24. Sharma S, Vyas S, Periasamy C, Chakrabarti P. Structural and optical characterization of ZnO thin films for optoelectronic device applications by RF sputtering technique. Superlattices Microstruct. 2014;75:378-389;Available from: https://doi.org/10.1016/j.spmi.2014.07.032.
25. Hong MH, Choi H, Shim D Il, Cho HH, Kim J, Park HH. Study of the effect of stress/strain of mesoporous Al-doped ZnO thin films on thermoelectric properties. Solid State Sci. 2018;82:84-91;Available from: https://doi.org/10.1016/j.solidstatesciences.2018.05.010.
26. Seetawan U, Jugsujinda S, Seetawan T, Ratchasin A, Euvananont C, Junin C, et al. Effect of calcinations temperature on crystallography and nanoparticles in ZnO disk. Mater. Sci. Appl. 2011;2:1302-1306;Available from: https://doi.org/10.4236/msa.2011.29176.
27. Pathak TK, Swart HC, Kroon RE. Influence of Bi doping on the structure and photoluminescence of ZnO phosphor synthesized by the combustion method. Spectrochim. Acta - Part A Mol. Biomol. Spectrosc. 2018;190:164-171;Available from:

https://doi.org/10.1016/j.saa.2017.09.026.
28. Whitmire KH. Bismuth: Inorganic Chemistry. Encyclopedia of Inorganic and Bioinorganic Chemistry 2004;Available from: https://doi.org/10.1002/9781119951438.eibc0018.pub2.
29. Le OKT, Pham ATT, Pham NK, Pham THC, Nguyen TH, Hoang DV, et al. Compensation of Zn substitution and secondary phase controls effective mass and weighted mobility in In and Ga co-doped ZnO material. J. Mater. 2021;7:742-755;Available from: https://doi.org/10.1016/j.jmat.2020.12.020.
30. Tanusilp S, Nishide A, Ohishi Y, Muta H, Hayakawa J, Kurosaki K. High thermoelectric power factor of ytterbium silicon-germanium. Appl. Phys. Lett. 2018;113:193901;Available from: https://doi.org/10.1063/1.5047091.
31. Snyder GJ, Toberer ES. Complex thermoelectric materials. Nat. Mater. 2008;7:105-114;Available from: https://doi.org/10.1038/nmat2090.
32. Guan W, Zhang L, Wang C, Wang Y. Theoretical and experimental investigations of the thermoelectric properties of Al-, Bi- and Sn-doped ZnO. Mater. Sci. Semicond. Process. 2017;66:247-252;Available from: https://doi.org/10.1016/j.mssp.2017.03.027.